

Asymmetric time sequence for multiple-exposure 3D PTV

Scarano, Fulvio; Hysa, Ilda; Grille Guerra, Adrian; Tuinstra, Marthijn; Sciacchitano, Andrea

DOI

[10.1007/s00348-025-03993-3](https://doi.org/10.1007/s00348-025-03993-3)

Publication date

2025

Document Version

Final published version

Published in

Experiments in Fluids

Citation (APA)

Scarano, F., Hysa, I., Grille Guerra, A., Tuinstra, M., & Sciacchitano, A. (2025). Asymmetric time sequence for multiple-exposure 3D PTV. *Experiments in Fluids*, 66(4), Article 74. <https://doi.org/10.1007/s00348-025-03993-3>

Important note

To cite this publication, please use the final published version (if applicable).
Please check the document version above.

Copyright

Other than for strictly personal use, it is not permitted to download, forward or distribute the text or part of it, without the consent of the author(s) and/or copyright holder(s), unless the work is under an open content license such as Creative Commons.

Takedown policy

Please contact us and provide details if you believe this document breaches copyrights.
We will remove access to the work immediately and investigate your claim.



Asymmetric time sequence for multiple-exposure 3D PTV

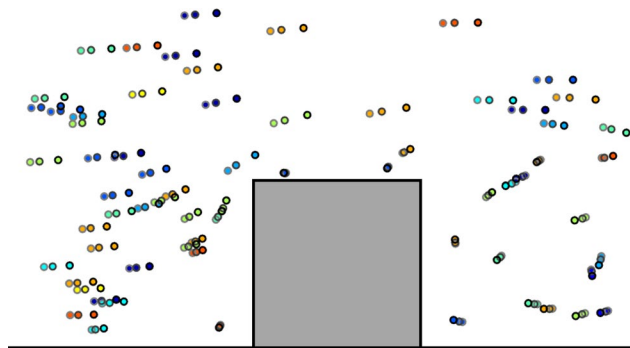
Fulvio Scarano¹ · Ilda Hysa^{1,2} · Adrian Grille Guerra¹ · Marthijn Tuinstra² · Andrea Sciacchitano¹

Received: 2 May 2024 / Revised: 28 December 2024 / Accepted: 2 February 2025
© The Author(s) 2025

Abstract

Recording onto a single-frame multiple exposures of the tracer particles has the potential to simplify the hardware needed for 3D PTV measurements, especially when dealing with high-speed flows. The analysis of such recordings, however, is challenged by the unknown *time tag* of each particle exposure, alongside their unknown organization into physical trajectories (*trajectory tag*). Using a sequence of two or more illumination pulses with a constant time separation leads to the well-known *directional ambiguity* problem, whereby it is not possible to distinguish the direction of motion of the tracer particles. Instead, an irregular and asymmetric sequence of time separation for the illumination pulses allows recognizing the *time tag* of the unique sequence of positions in the image, composing the *trace*. A criterion is formulated here that recognizes unambiguously the *trace* pattern, based upon the principle of kinematic similarity. A combinatorial algorithm is proposed whereby a signal-to-noise ratio is introduced for every candidate trace. The approach is combined with an additional criterion that favors trace regularity (minimum velocity fluctuations). The algorithm is illustrated making use of particle motion examples. Furthermore, it is assessed using 3D experimental data produced with time-resolved analysis (single-frame, single-exposure) using the *Shake-the-Box* method. Traces with a three-pulse sequence yield a detection rate of 85%. The latter declines with the number of pulses. Conversely, the error rate rapidly vanishes with the samples number, which confirms the reliability of trace detection criterion when more pulses are comprised in the sequence.

Graphical abstract



1 Introduction

With the advent and diffusion of 3D velocimetry techniques, we are witnessing a rapid transition from the PIV measurement mode (high image density, cross-correlation motion analysis, double-frame recordings) toward the PTV mode (low image density, particle detection and pairing, multi-frame recordings). Numerous clear advantages are at the basis of such transition (see, for instance, the work from Kahler et al. 2012a, 2012b, 2012, and Cierpka and Kahler,

✉ Fulvio Scarano
f.scarano@tudelft.nl

¹ Department of Aerospace Engineering, TU Delft, Delft, The Netherlands

² Vertical Flight and Aeroacoustics Department, Dutch Aerospace Center, Amsterdam, The Netherlands

2012, among others), which is not expected to be reversed, but further accomplished due to the advancement of high-quality scientific imagers (e.g., sCMOS), highly scattering tracers (e.g., HFSB, Bosbach et al. 2009), safer and more versatile volumetric illumination devices (e.g., LED, Willert et al. 2010) and not least, more advanced algorithms for the particles motion analysis.

State-of-the-art three-dimensional particle tracking is founded on the iterative 3D particle detection method (IPR, Wieneke 2012). Particle pairing, initially based on predictor–corrector techniques (Malik and Drakos, 1993), has been profoundly revised and coupled within the image processing analysis, resulting in a powerful and computationally efficient method (Shake the Box, Schanz et al. 2016). Most of the current research focuses on single-pulse, double- or multi-frame recordings, which requires high-speed illumination and imaging for the latter. Techniques based on multiple-exposure analysis have been practiced in conjunction with the photographic PIV recording technique, but rapidly declined with the advent of kilohertz rate illumination and imaging systems (Raffel et al. 2018). The recording and analysis of streaks, obtained with long-pulse illumination, have also been practiced, and a recent review article surveys developments of particle streak velocimetry (Zhang et al. 2024).

The main motivation for using single-frame ME recording relates to the simplicity of the hardware required. Furthermore, the latter may become relevant, again, in view of developments toward multi-camera redundant systems (Hysa et al. 2024; Wieneke and Rokstroh, 2024; Hendriksen et al. 2024), where a multitude of imagers need to be employed. Furthermore, time-resolved analysis of particle motion requires increasingly high imaging rates when aerodynamic flows at velocity higher than 10 m/s are to be investigated. In those situations, one reverts to double-frame recording, to detriment of the velocity dynamic range (Lynch and Scarano, 2013), unless one combines multiple measurements with different pulse separation using a predictor–corrector approach (Saredi et al. 2020).

ME recording can potentially solve the above trade-off, provided that the information lost in the single-frame recording (particle image *time tag*) can be restored in some way.

The analysis of ME recordings has been and still remains an open, challenging problem, due to the strong ambiguity of the time tag of particles images all featuring identical properties. For instance, Utami and Ueno (1984) performed a manual analysis of four-pulse recordings (Fig. 1). Yet, the direction of motion needed to be determined by additional criteria (Adrian and Westerweel, 2011). Early works dealt with planar illumination, mostly, and the problem of truncated traces by out-of-plane motion was approached using a dot–streak–dot encoding of the particle image (Agüí and Jimenez, 1987). A solution to the problem of directional ambiguity was proposed by Grant and Liu (1990), with the pulse tagging technique, whereby the preceding and following pulses were differing in intensity. Qureshi and Tien (2022) and most recently Zhang et al. (2024) illustrated techniques for streak analysis. Yet, a conclusive statement is missing on how to address the directional ambiguity in a systematic way and demonstrate the principle beyond planar experiments.

A specific development of the Shake-the-Box technique for double-exposure recordings has been proposed, whereby a total of four exposures are collected on a double-frame recording. The directional ambiguity is approached here making use of either a tentative search or making use of a particle–space correlation to produce a statistical velocity predictor (Novara et al. 2019).

In conclusion, for a multiply exposed recording, the two main problems are the *time tag* determination (i.e., establishing the correspondence of each dot or 3D particle sample to a time instant) and the *trajectory tag* assignment (i.e., associating multiple particle samples to the same physical tracer and defining its trajectory). The latter also exists for single-exposure systems and is more commonly known as the particle image *pairing* problem. When the density of particle images in the recording is increased such that the distance between particle occurrences falls below their traveled path between pulses, the probability of incorrect pairing grows exponentially, as discussed in the early works on PTV (Maas et al. 1993, among others). Finally for 3D measurements, for a given concentration of the tracers, recording multiple positions of the particle tracers on a single image increases the image density and the associated probability of ghost

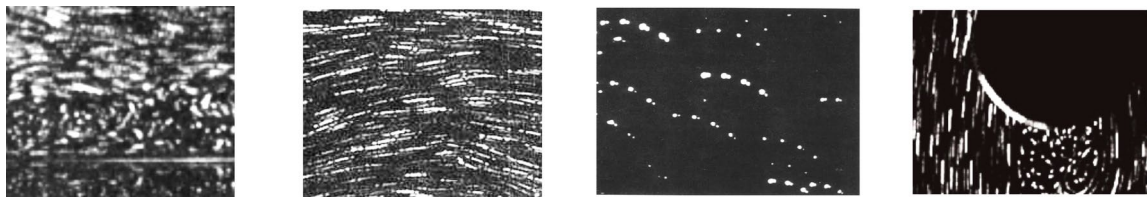


Fig. 1 Examples of ME recordings for PTV analysis of fluid flows. From left to right: four-pulse (repr. from Utami and Ueno, 1980); pulse–streak–pulse (repr. from Agüí and Jimenez, 1990); pulse tag-

ging (repr. from Grant and Liu 1990); streak velocimetry (repr. from Qureshi and Tien 2022)

particles. An additional problem of ME recordings is the overlap of exposures from the same particle, when traveling at vanishing velocity. This has been approached brilliantly for planar measurements with image-shifting devices (Landreth and Adrian, 1988). Extension of the method to 3D systems, however, is deemed of formidable complexity.

The present study examines the problem of *time-tag* and *trajectory-tag* determination for multiply exposed recordings. The principle to resolve the directional ambiguity is that of sequence tagging, i.e., a specific temporal sequence is utilized, where the time intervals are irregular and do not exhibit time symmetry. The result is an irregular sequence of dots, here called a *trace*, to be compared to the imposed sequence of illumination. This principle has been explored by Hysa et al. (2022), who examined the impact of the sequence structure on the trace detectability. In the present work, a concept from cross-correlation analysis used in PIV is borrowed: the signal-to-noise ratio, which enables detecting a trace as a whole. This principle is applied here to a cost function (similar to the pixels product in cross-correlation) applied to candidate sequence of dots. The similarity between the time sequence and the spatial occurrence of dots is invoked as the *kinematic similarity* criterion that recognizes the trace as a sequence of dots along the particle trajectory (*trajectory tag*) and resolves the directional ambiguity of said dots (*time tag*).

An additional constraint on particle acceleration (*trace regularity*) is adopted and combined with the latter to yield a composite signal-to-noise ratio.

The working principle is first illustrated with some simplified examples and then demonstrated, using an experimental database of 3D time-resolved measurements around a wall-mounted cube immersed in a turbulent boundary layer at $Re = 80,000$ (Hendriksen et al. 2024).

2 Some definitions

Let us consider a tracer particle moving along its trajectory Γ . Light is scattered by the tracer when subject to N illumination pulses separated with known time intervals, with N denoted as the sequence rank. Such sequence of illumination pulses is denoted as *temporal template* $\tau = \{t_1, t_2, \dots, t_N\}$, with $t_1 = 0$ and $t_N = T$, the latter being the duration of the entire sequence. We indicate the normalized vector of time instants as $\tau^* = \tau/T$. It follows that $\tau^* \in [0, 1]$. Figure 2 illustrates temporal templates and the corresponding normalized time of pulses, with some choices for a sequence or rank 4, with a uniform time separation (left), or non-uniform, yet time-symmetric (middle) and fully asymmetric (right).

As discussed in Hysa et al. (2022), the structure of the sequence is of importance to resolve the directional ambiguity. A symmetric sequence of pulses cannot disambiguate the direction of motion because the particle can be interpreted as traveling forward as well as backward, with origin at $n = 1$ or $n = 4$, respectively (Fig. 2 left). The same can be said for the non-uniform example (Fig. 2 middle).

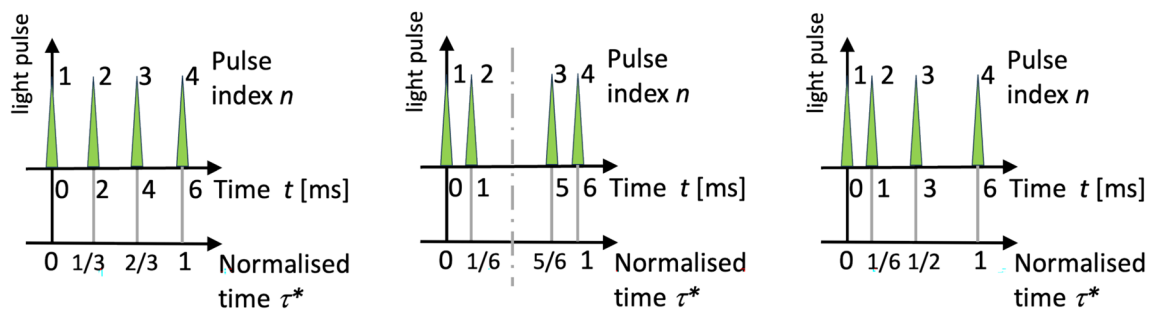
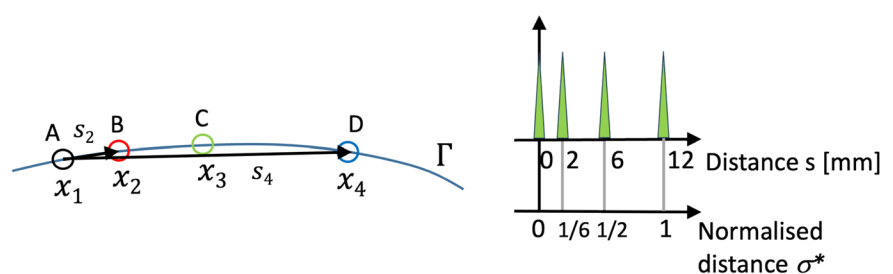


Fig. 2 Examples of temporal templates of four-pulse sequences. Uniform time separation (left); non-uniform but symmetric (middle); asymmetric sequence (right)

Fig. 3 Examples of spatial pattern, or *trace*, produced by a particle illuminated with asymmetric four-pulse sequence (left). Diagram of distance from first dot (right)



Let us define the particle trajectory Γ (Fig. 3 left). Once the particle tracer is illuminated with a pulse sequence, a spatial pattern, or *trace*, \mathfrak{T}_N is formed in the image, with dots (viz. marks) placed at a traveled distance from the first dot that corresponds with the elapsed time. The spatial arrangement of dots depends upon the temporal template, alongside the velocity and the acceleration of the tracer along the trajectory.

Let define the marks' position vector by $\mathbf{X}_p = \{\mathbf{x}_1, \mathbf{x}_2, \dots, \mathbf{x}_N\}$ for \mathfrak{T}_N . Correspondingly, we indicate the vector of traveled distance as $\sigma = \{s_1, s_2, \dots, s_N\}$ with $s_n = \mathbf{x}_n - \mathbf{x}_1$. It follows that $s_1 = 0$ and s_N approximates the path length. It follows that $s_N \sim \bar{V} \cdot T$ where \bar{V} is the average particle velocity along Γ . The normalized abscissa is $\sigma^* = \sigma/s_N$, resulting into $\sigma^* \in [0, 1]$.

Figure 3 right shows the distance traveled by the particle during the illumination sequence. It is taken in this case the asymmetric sequence, for example.

For 3D imaging systems, the pattern and the distance traveled also depends upon the viewing direction. The current discussion is exemplified here in two dimensions with no loss of generality and extended to three dimensions in the section presenting the experimental results. It is worth mentioning that once the particle position is reconstructed in 3D space, the dot sequence is turned in a sequence of particle samples and the effect of the viewing direction is eliminated.

3 Trace detection principle

3.1 Kinematic similarity

In the hypothesis that the particle tracer travels at approximately uniform and rectilinear velocity, the spatial pattern of dots \mathfrak{T}_N will exhibit similarity with the temporal template. In other terms, the traveled distance will be proportional to the elapsed time and their normalized counterparts τ^* and σ^* should obey the criterion of *kinematic similarity* (KS):

$$\varepsilon_{\sigma\tau} = \left\{ \sum_{n=1}^N \left[(\sigma_n^* - \tau_n^*)^2 \right] \right\}^{1/2} = 0 \quad (1)$$

The above equation appears as a definition. However, the pulse index n is only known for τ^* , not for σ^* . Therefore, for a chosen set of N dots, the KS criterion needs to be evaluated for all possible choices of the pulse index (here also refereed as the *time tag*), which corresponds to $N!$ permutations of the index.

The situation is illustrated in Table 1, for a three-pulse sequence of normalized time template $\tau^* = \{0, 1/3, 1\}$, where the order of the time tags (A–B–C) is varied according to the permutations, each corresponding to a possible path. It is assumed that the trace marks are placed at distances $\sigma = \{0, 2, 6\}$ mm (uniform rectilinear motion).

The first column yields the order of the combination according to the pulse number (1–2–3). For instance, the permutation B–A–C selects the second exposure (B) as origin of the trace and the third exposure (C) as the end of it. The following three columns represent the distance from the chosen first mark. The following three columns yield the same distance but normalized with respect to the path length s_3 .

By definition, the normalized distance is null for the first mark and of unit value for the last. However, the distance of the intermediate mark can vary widely along the permutation.

Evaluating Eq. 1 for these combinations yields the disparity of the trace from kinematic similarity $\varepsilon_{\sigma\tau}$, (see last column of Table 1). In the present case, the correct order pertains to the permutation A–B–C, yielding $\varepsilon_{\sigma\tau} = 0$. All other permutations return nonzero value, to confirm that the current method does not suffer from directional ambiguity. It is worth mentioning that for a symmetric temporal template (like in Fig. 2 left and middle), a second permutation, C–B–A also yields $\varepsilon_{\sigma\tau} = 0$, introducing the directional ambiguity.

In most flow fields of interest, the velocity of a particle tracer does exhibit variations along the trajectory. Therefore, the hypothesis of uniform rectilinear motion does not hold true, rendering the KS criterion not usable when

Table 1 Combinatorial of distance, normalized distance and KS residual of a three-pulse trace

Trace	Order	Distance [mm]			Normalized distance			KS
	1–2–3	s_1	s_2	s_3	s_1^*	s_2^*	s_3^*	$\varepsilon_{\sigma\tau}$
	A–B–C	0	2	6	0	1/3	1	0
	A–C–B	0	6	2	0	3	1	8/3
	B–A–C	0	2	4	0	1/2	1	1/6
	B–C–A	0	4	2	0	2	1	5/3
	C–A–B	0	6	2	0	3	1	8/3
	C–B–A	0	4	6	0	2/3	1	1/3

applied strictly according to Eq. 1. Yet, for any given set of N marks, a detection criterion for the trace \mathfrak{F}_N can be based on finding the condition of minimum value for $\varepsilon_{\sigma\tau}$ across the combinatorial set:

$$\min_{\mathfrak{F}} \{ \varepsilon_{\sigma\tau} \}_K, \quad (2)$$

where K is the number of possible permutations from the N considered particle images ($K=N!$).

Here a concept is borrowed from the theory of cross-correlation analysis of PIV images: The condition where all particle positions coincide in the image pair yields a correlation maximum and the position of such peak corresponds to the velocity of the particles enclosed in the window. When normalized, the height of the correlation peak, relative to the secondary ones, depends upon the number of particle image pairs (Keane and Adrian 1992). A commonly used detection criterion for a valid vector is based on the ratio between the highest and second-highest peak in the correlation map.

In a similar way, the combinatorial analysis yields a set of values for the KS criterion. Here, the ratio between the second-lowest value and the minimum value of $\varepsilon_{\sigma\tau}$ is taken as indication of signal-to-noise ratio (SNR).

$$\text{SNR}_{\sigma\tau} = \frac{2^{\text{nd}} \min \{ \varepsilon_{\sigma\tau} \}}{\min \{ \varepsilon_{\sigma\tau} \}} \quad (3)$$

The above definition yields $\text{SNR}_{\varepsilon_{\sigma\tau}} \rightarrow \infty$ when the minimum of $\varepsilon_{\sigma\tau}$ is null. This condition, however, does not occur in real experiments, where the effects of spatiotemporal velocity variations and measurement noise render $\min \{ \varepsilon_{\sigma\tau} \}$ nonzero.

3.2 Trace regularity

The KS criterion is defined from a scalar equation and cannot distinguish between rectilinear and non-rectilinear paths. For that purpose, a criterion based on the variations of the velocity vector direction and magnitude is devised, as also frequently adopted in the literature for PTV analysis. The acceleration is estimated along the trace piecewise. The criterion is named after *trace regularity* (TR) and reads as:

$$\min_{\mathfrak{F}} \{ \varepsilon_{\alpha} \}_K, \quad (4)$$

Here ε_{α} is defined as the sum of the standard deviation from each component of the velocity vector along the trace. An example that applies this criterion is given in Table 2, for the simplified case of a three-pulse trace along a rectilinear trajectory.

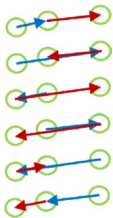
The combination yields a similar result as for KS; however, the two criteria do not repeat the same ranking in terms of their residual. For KS, the second-lowest residual corresponds to the sequence B–A–C, whereas for TR the sequence C–B–A yields the second-lowest residual. The above circumstance proves that the two criteria are not redundant and provide complementary analysis, suited to trace detection.

Following the same approach proposed for KS, the ratio between the second-lowest value and the minimum value of ε_{α} is taken as indication of signal-to-noise ratio (SNR_{α}).

$$\text{SNR}_{\alpha} = \frac{2^{\text{nd}} \min \{ \varepsilon_{\alpha} \}}{\min \{ \varepsilon_{\alpha} \}} \quad (5)$$

The two signals are defined in the same combinatorial space and can be superimposed through their product $\prod \varepsilon = \varepsilon_{\sigma\tau} \cdot \varepsilon_{\alpha}$ (composite residual), reported in the last column of Table 2. The composite residual is defined in the space of particle time-tag permutations and sets the basis for a general definition a

Table 2 Combinatorial of velocity and its variation for a three-pulse trace

Trace	Order	Velocity [m/s]			$\varepsilon_{\sigma\tau}$	ε_{α}	$\Pi\varepsilon$
	1–2–3	v_1	v_2	$ \Delta v $			
	A–B–C	6	6	0	0	0	0
	A–C–B	18	–6	24	8/3	24	64
	B–A–C	–6	9	15	1/6	15	2.5
	B–C–A	12	–9	21	5/3	21	35
	C–A–B	–18	3	21	8/3	21	56
	C–B–A	–12	–3	9	1/3	9	3

trace detection criterion (TD) that combines kinematic similarity and trace regularity:

$$\min_{\mathfrak{S}} \left\{ \prod \varepsilon \right\}, \quad (6)$$

The value of the residuals corresponding to the correct sequence in this example is zero, given that ideal conditions considered (no noise and zero acceleration). In realistic condition, an estimate of such minimum can be estimated in the order of typically $o(0.1)$, when considering the combined effect of measurement and trajectory modeling uncertainties altogether not exceeding 10%. When the two criteria are multiplied, the composite criterion is expected to yield a minimum in the order of 10^{-2} . The spurious permutations, instead, yield values of unit order or larger. As a result, the signal-to-noise ratio of the composite criterion is expected in the order of 100 or above, which indicates a favorable condition in terms of trace detectability. The above is corroborated by some numerical examples.

3.3 Numerical assessment

With the purpose to illustrate the principle of the algorithm, a simplified numerical example is presented here, with typical categories of flow motions and particle image occurrence being considered.

3.3.1 Uniform circular motion

A first category of particle motion is that of non-rectilinear trajectory. Here the simplified condition of uniform circular motion is considered, which may occur, for instance around the core of a vortex. The trace has its origin at the point $(X, Y) = (10, 0)$ mm, with the particle traveling (counterclockwise) along a circle of radius $R = 10$ mm. The case is parametrized in terms of the particle path $s(t) = V t$, ($V = \omega R$), where ω is the angular speed, expressed in rad/s. Figure 4 illustrates the three conditions, namely $s(T) = \{\pi R/4, \pi R/2, \pi R\}$ ($1/8, 1/4$ and $1/2$ circle, respectively). Up to a path encompassing $\pi R/2$, the TD identifies the correct sequence order with a good level of confidence ($\text{SNR} > 6$). When the angular range is increased to $2\pi R/3$, the detection remains correct, but SNR drops below 3, which is taken here as a limit condition. Finally, for a trace encompassing a half circle the method fails and it yields the incorrect sequence order.

Furthermore, Fig. 4 illustrates the separate distribution of residual (inverted for clarity) of kinematic similarity and trace regularity for each value of the permutation index k . It can be noticed that the highest value corresponds to the same index, but the clouds of the spurious values vary for the two

criteria, which generally produces a higher SNR when their combination is considered.

3.3.2 Rectilinear motion with uniform acceleration

A similar analysis is made for the rectilinear motion with uniform acceleration. In this case, the equation of motion reads as $s(t) = V t + \frac{1}{2} a t^2$. With a being the acceleration. Here the parameter of importance is the maximum velocity variation, normalized by the mean velocity $\Delta V/\bar{V}$. Two conditions are illustrated in Fig. 5, with values taken from the experimental conditions presented in the remainder. In case of mild acceleration ($V = 10$ m/s and $a = 100$ m/s², $\Delta V/\bar{V} = 0.02$), a correct detection is obtained with $\text{SNR} \sim 10^3$. In a region of rapid deceleration (stagnation, $V = 5$ m/s and $a = -500$ m/s², $\Delta V/\bar{V} = 0.20$), the detection is still possible, yet with lower confidence ($\text{SNR} = 7$). For even higher values of the acceleration ($\Delta V/\bar{V} > 0.25$), the SNR falls below 3 and the incorrect order is given for the considered trace.

3.3.3 Neighboring trajectories

In real experiments, traces from different particles will occur at some proximity. As a consequence, for a selected region of space, the search for a group of particle samples composing a trace will frequently include additional particle samples from other traces. Here the task of the detection algorithm is to identify those belonging to a specific trace unequivocally (*trajectory tag*).

Figure 6 illustrates two conditions: On the left, the marks from another (incomplete) trace lie at some distance from the trace, whereas on the right, they appear as intersecting and may be more easily confused with it.

The evaluation of the detection criteria is shown in Fig. 7. The top row displays the evaluation of the red trace on the left of Fig. 6. The first column displays the residual of the kinematic similarity, the second is the trace regularity and in the third column their produce (composite criterion).

In this case, the four marks composing the trace are selected correctly, given that the spurious marks are sufficiently apart. The criteria are evaluated for all 24 permutations ($4!$) of such four marks. It can be observed that the separation between best and second-best choice for KS and of TR is in the order of 10 and 100, respectively. The composite criterion is therefore a separation (i.e., SNR) exceeding 10^2 .

The situation on the right of Fig. 6 features the spurious marks (green) in close proximity of the main trace (in red). In this case, the four marks selected for the analysis

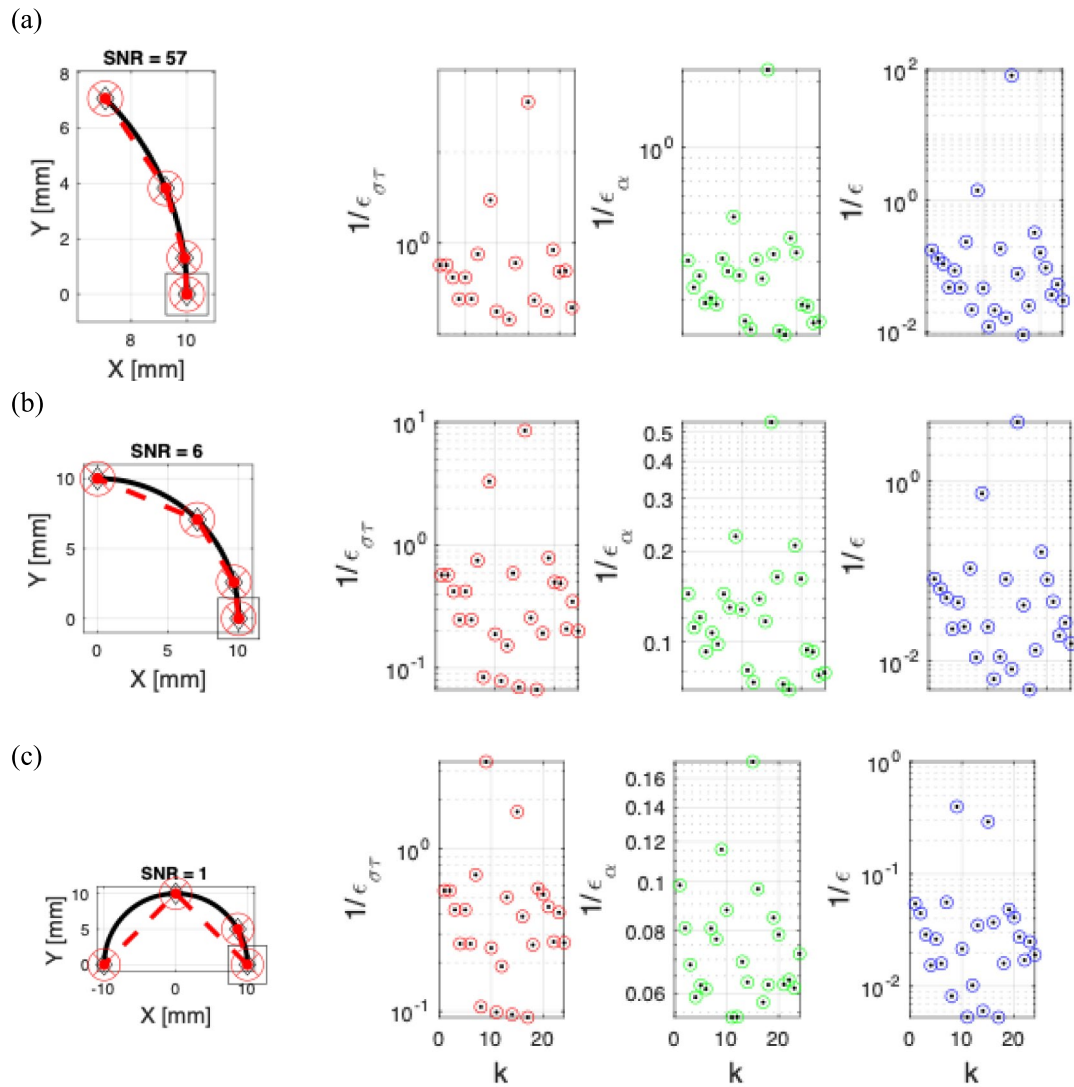


Fig. 4 Left: trace detection from uniform circular motion with paths of increasing angular range ($\pi R/4$ (a), $\pi R/2$ (b) and πR (c)). The first exposure (origin) is labeled with a square, the actual trajectory

in solid black line and trace segments with red dashed line. Right: inverted residual of KS, TR and composite

contain one spurious mark and the results are shown in the bottom row of Fig. 7. Both KS and TR exhibit a minimum in the unit order of magnitude alongside the composite criterion SNR being of unit order. The latter informs that the selected set of marks does not belong to a physical particle trajectory and the trace should be rejected.

In the latter example, the importance of preselecting the sets of marks to form a trace is emphasized. From combinatorial analysis, the number of possible permutations of M marks by groups of N ($M=7$ and $N=4$ in Fig. 7) is given by:

$$P = \binom{M}{N} = \frac{M!}{(M-N)!N!} \quad (7)$$

It should be retained in mind that the value of P increases very rapidly with M . Thus, any algorithm using this approach requires a careful choice of the minimum neighborhood for trace evaluation. In the absence of additional criteria that limit the selection of the samples, it is therefore necessary that the number of marks considered to identify a trace are taken in relatively small subgroups by preselection (e.g., $M < 10$ and $N < 5$). For every candidate trace, the detectability criteria need to be evaluated for every permutation of the time tag, with a total of $K = N!$ permutations, as illustrated in Fig. 2, with $N=3$ and $K=6$. Combining both requirements returns a total number of evaluations Q that reads as:

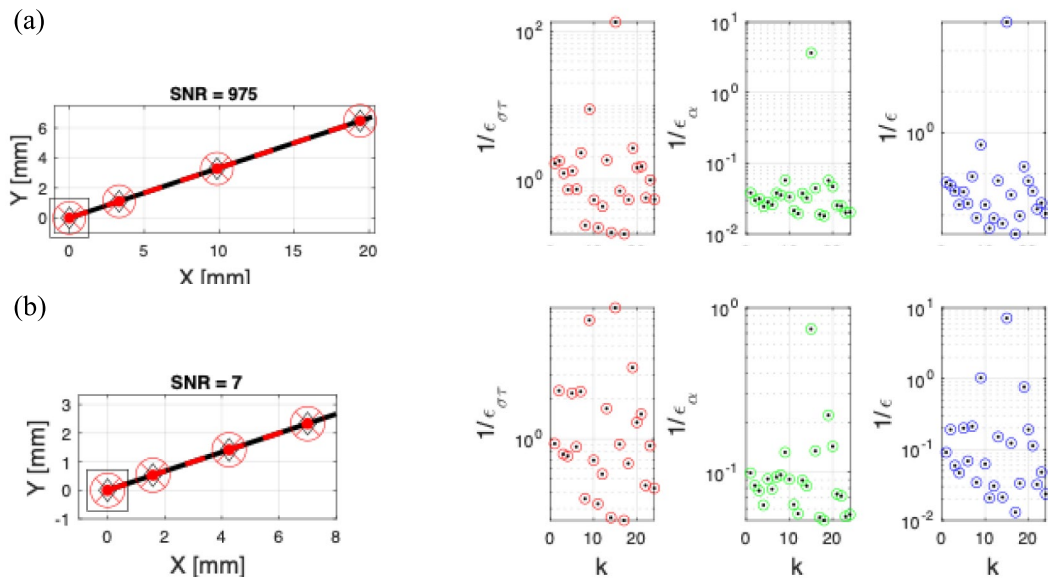


Fig. 5 Trace detection from uniformly decelerated motion (left). Residual (inverted) of kinematic similarity, trace regularity and composite criteria (right). $|\Delta V/\bar{V}|=2\%$ (a) and 20% (b)

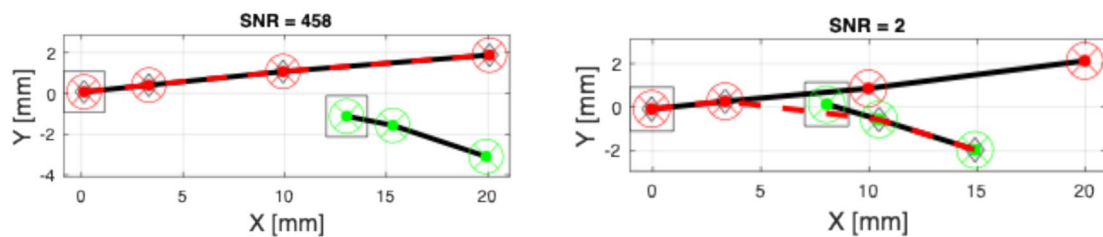
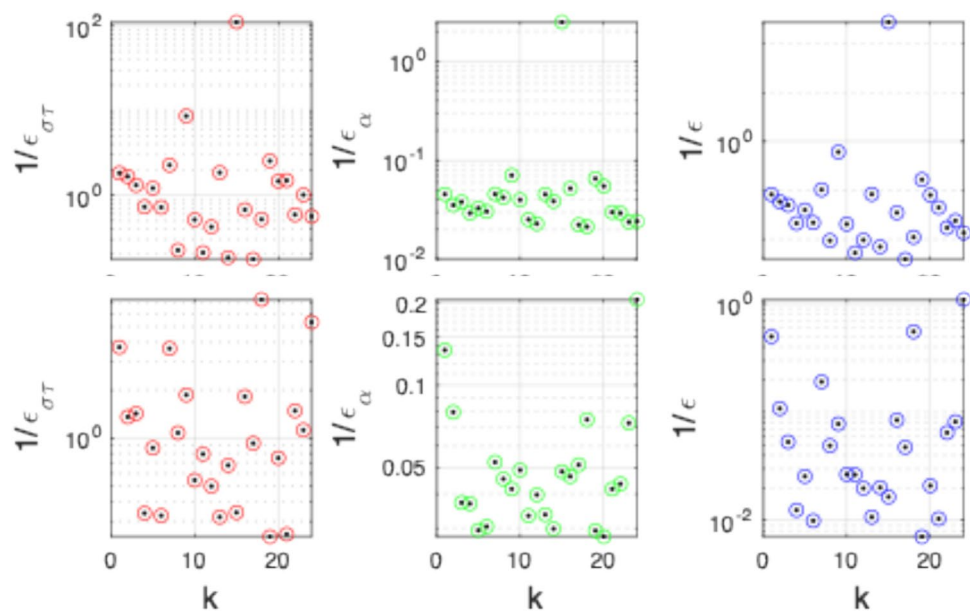


Fig. 6 A set of 7 candidate particle samples, of which 4 pertain to a trace (red labels) and 3 are from an incomplete, truncated, trace (green labels). Left: distance between traces is sufficiently large to detect the correct trace. Right: interference and spurious trace detection

Fig. 7 Values of inverted KS residual ($\epsilon_{\sigma T}$, left), TR residual (ϵ_{α} , middle) and their product (right) as a function of particle permutation within a set. Top row corresponds to Fig. 6 left, where all selected marks belong to a physical trace. The bottom row corresponds to Fig. 6 right, where marks from a nearby spurious trace are included in the quartet, failing the trace detection



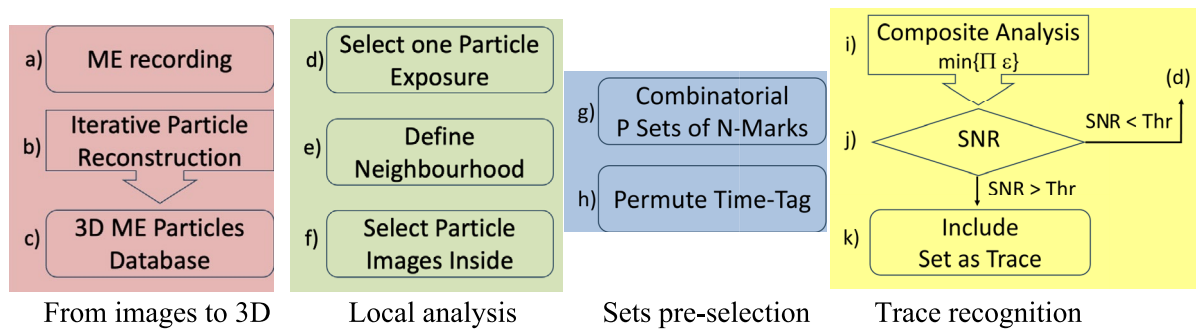


Fig. 8 Flowchart describing the main operations of the *trace* algorithm. Main blocks highlighted in the lower row

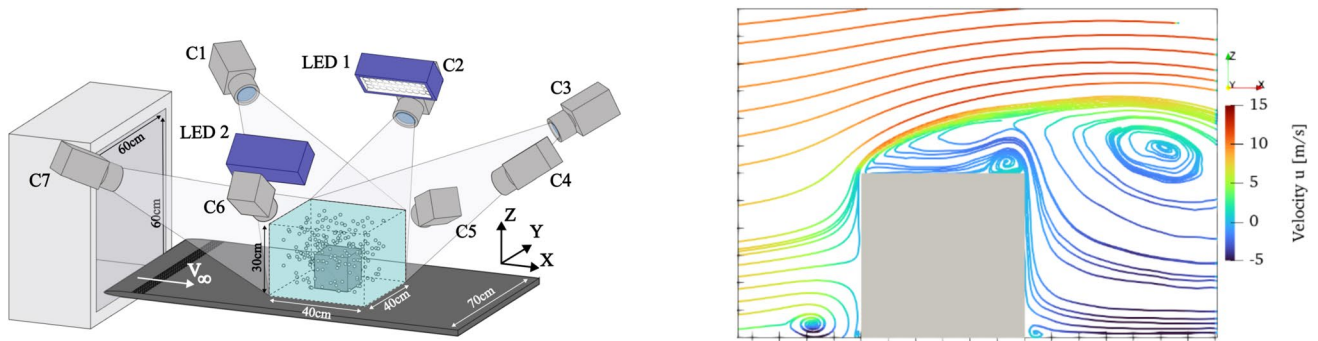


Fig. 9 Left: experimental arrangement and layout of the 3D particle tracking system. Right: time average, velocity color-coded, streamlines pattern in the median plane (tick marks are spaced by 2 cm)

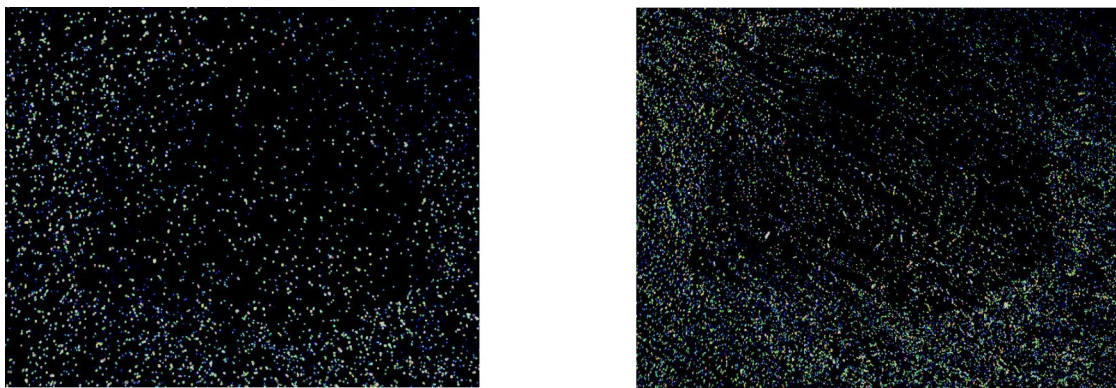


Fig. 10 Images of HFSB tracers from a single (left) and triple exposure recorded from one of the seven cameras. Exposures at $\tau = \{0, 0.33, 1\}$ ms

$$Q = PN! = \frac{M!}{(M-N)!N!} N! = \frac{M!}{(M-N)!} \quad (8)$$

Due to the associated computational burden, methods that reduce the complexity of both the candidate trace selection and time-tag permutation are needed to make this approach affordable. Some approaches have been explored and their effect on

the computational time are discussed in Sect. 6 (Figs. 8, 9, 10, 11, 12, 13, 14 and 15).

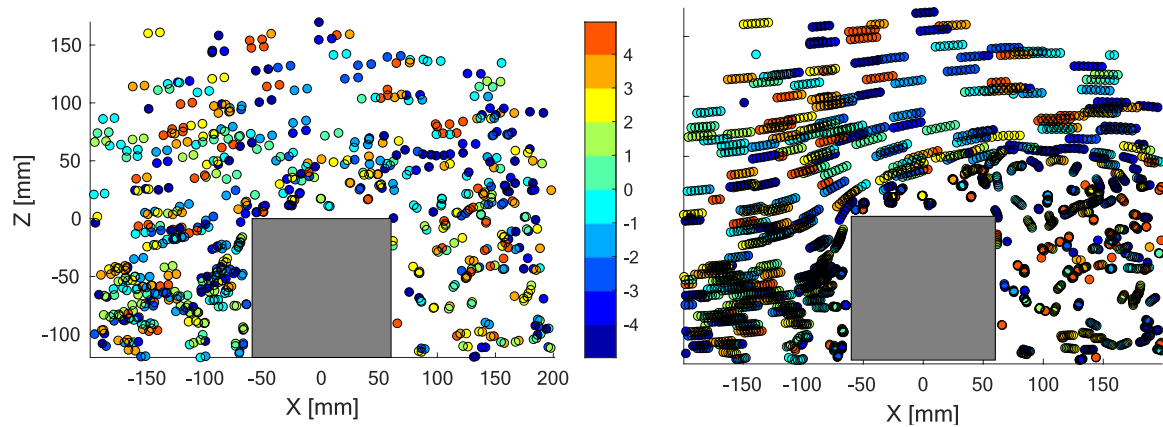


Fig. 11 3D particles positions from the experimental database. Color coded depth position (in mm). Left two time instants separated with 1 ms. Right: six time instants with 0.33 ms uniform time separation. Direction of motion is ambiguous, due to the choice of uniform pulse separation

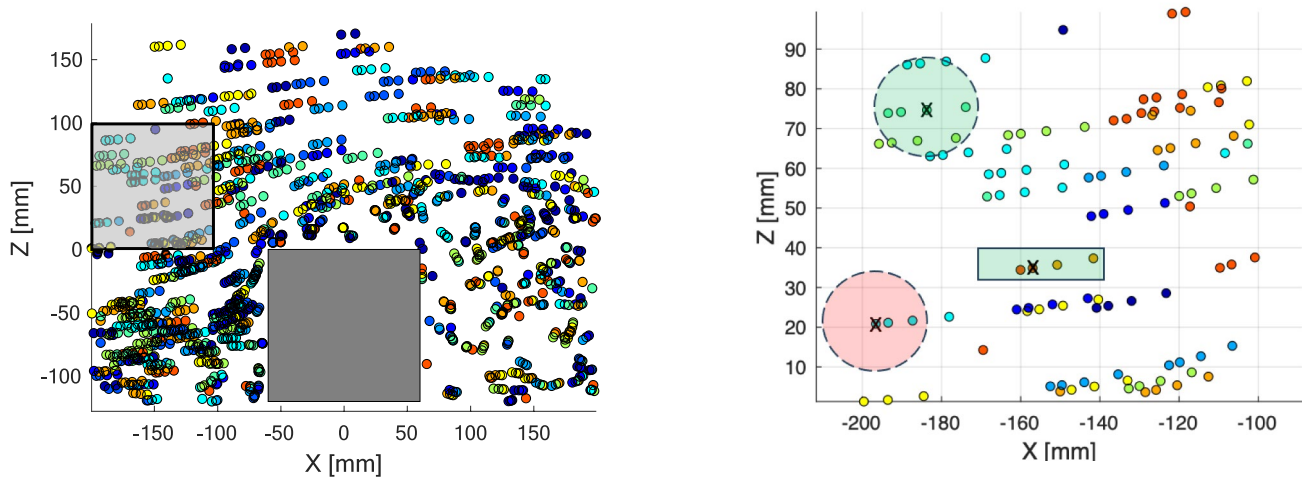


Fig. 12 Particles positions from the experimental database. Color coded depth position (in mm). Left: Four-exposure recording with irregular (increasing) time separation. Right: zoomed view from the shaded square in the left picture Isotropic (circles) and adapted (rec-

tangle) neighborhoods are shown. The green color indicates that all exposures from the trace are captured. The red color indicates incomplete set of exposures

4 Numerical algorithm

The above principles are implemented in a numerical program, schematically depicted in Fig. 8 and video-illustrated with an animation file appended as supplementary material. The process considers as input the recording of multiply exposed images of particles (box *a*) such as illustrated in Fig. 9 right. Particle image triangulation (e.g., IPR, box *b*) yields 3D particle positions, at unknown time instants (box *c*), of which an example is illustrated in Fig. 8. The algorithm interrogates particle exposures selecting them one after the other (sequential, box *d*). A

search region is chosen around the exposure (box *e*), based either on the maximum expected velocity or a local estimate of the velocity, when available (Fig. 10 right), and the total time elapsed between the first and the last pulse. The minimum search diameter d_s must include the entire trace, which turns into the condition that $d_s \geq \bar{V}T$. In this case, when marks at the edge of a trace are selected, the search region does not include the whole trace and the search fails. When a mark in the middle of the trace is considered, the search region includes the whole trace, which may be detected if it obeys the composite detection criterion. This is schematically illustrated in Fig. 11 right.

Fig. 13 Particle selection and trace detection in a sample region. Top left: particles and velocity vectors from the STB analysis. Top right: selected particles (denoted by a black cross) that do not lead to a trace because their neighborhood does not include enough samples. Bottom left: when a particle's neighborhood contains sufficient samples, the set is subject to the composite detection criterion. Two traces are detected (around the large-circled particle), of which one is erroneous (in red). Bottom right: the process advances for all the particles. Most errors occur in regions of nearly overlapping traces

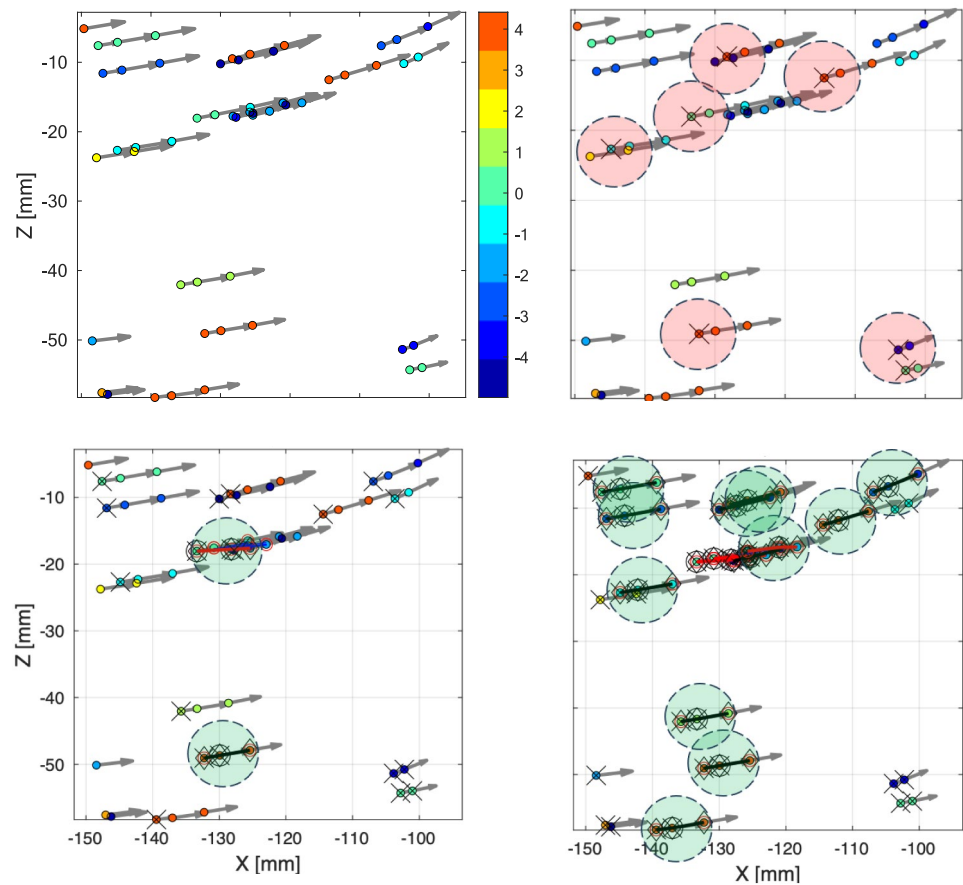


Fig. 14 Left: three-pulse sequence temporal template and the corresponding trace (bottom). Middle: search region and neighborhood around the selected mark. Right: linear fit evaluation of all trace possibilities, with the residuals shown in red

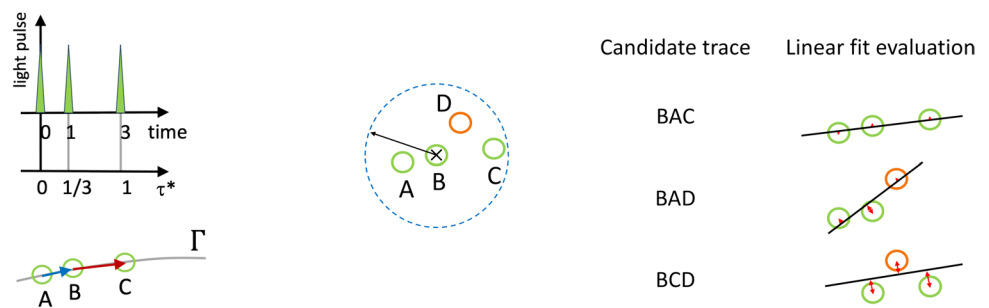
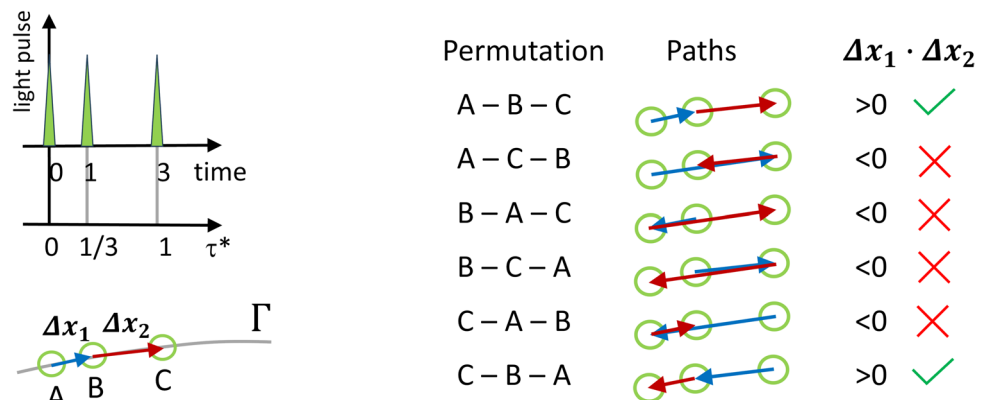


Fig. 15 Left: three-pulse sequence temporal template and the corresponding trace (bottom), together with the displacement vector Δx_1 and Δx_2 . Right: time-tag permutation list, corresponding paths (blue for the first displacement and red for the second one), direction disambiguation and output of the detectability criteria for the appropriate permutations



Assuming that M marks fall within the search region (box f) around the selected mark, the combinations with $N-1$ candidate marks is considered (each group of N marks must include the selected mark too). All combinations of $M-1$ marks by groups of $N-1$ are considered (box g).

For each combination, all possible time-tag permutations are considered (box h , see also Fig. 11 right), over which the TD criterion from Eq. 6 is applied (box i). The value of the SNR with respect to a chosen threshold value (box j) determines accepting the set as a trace (box k) or discarding it and move back (to box d). The process terminates when all particle exposures have been considered or assigned. As for many interrogation techniques, the method can be imagined with a single pass or by multiple iterations, where some parameters (search diameter, SNR threshold) are varied along the iterations. For sake of conciseness, variants of the algorithm are not discussed here.

5 Experimental database

Experiments are conducted in the W-tunnel, a low-speed open jet facility at the aerodynamics laboratories of the Aerospace Engineering Department of TU Delft. A cube of side length 12 cm is installed on a flat plate immersed in a stream at 10 m/s. A turbulent boundary layer develops along the plate with approximately 2 cm thickness. The cube Reynolds number is $Re_h = 80,000$ where h is the cube height. The flow is seeded with helium filled soap bubbles (HFSB, neutrally buoyant, 300 μm median diameter) released by a 200-generator seeding rake integrated in the wind tunnel (Jux et al. 2020). The tracers' concentration is approximately 1 bubble/ cm^3 . The layout of illumination and imaging systems is shown in Fig. 10: two *LED-Flashlight 300* arrays from LaVision produce pulsed illumination at a rate of 3 kHz. Seven high-speed CMOS cameras (Photron *FastCam SA-I*, 1 Mpx, 5400 fps, 12 bits) capture the light scattered by the HFSB tracers. The 7 cameras are distributed with their view such to cover the entire object and the flow field around it, to study accurate object position registration (Hendriksen et al. 2024) and its integration within the 3D particle tracking measurement (Wieneke and Rockstroh 2024). The whole volumetric dataset encompasses a domain of $40 \times 40 \times 30 \text{ cm}^3$. Ground-truth data are obtained making use of the Lagrangian Particle Tracking *Shake-the-Box* algorithm (available in the LaVision DaVis 10 software) for the full time-resolved sequence. In the above database, the particles position is measured every 333 μs and the trajectory tag (also known as track ID) is known from the STB algorithm. The particle positions measured every 333 μs are under-sampled skipping some pulses, to simulate the asymmetric sequence of pulses. This approach allows a direct comparison of the trace detection algorithm with the ground

truth provided by the single-exposure, time-resolved analysis performed with STB. For the present analysis, a 4-cm-thin slab of particles position data is considered and the data domain encompasses the (X, Y, Z) range $([-15, 20], [-2, 2], [-12, 12]) \text{ cm}^3$, respectively.

It is worth mentioning that the current assessment begins directly from the particle positions (box c in Fig. 8). This is chosen to avoid that the effect of ghost particles and missed detections due to particle image overlap play a role in the comparison. As a matter of illustration, Fig. 12 compares the original (single-exposure) particle image recording (left) and that obtained summing up four exposures (right) in a sequence of pulses at $\tau = \{0, 0.33, 1.0, 2.0\} \text{ ms}$.

As mentioned above, the current analysis is performed simulating the ME recordings and analyzing directly the reconstructed 3D position of particles. Figure 12 presents the 3D particle tracers positions for the case of 2 and 6 exposures recording with uniform time separation, to illustrate the problem of directional ambiguity.

6 Results

In Fig. 11, the example of a four-pulse single-frame recording is shown, according to the time instants sequence $\tau = \{0, 0.33, 1.0, 2.0\} \text{ ms}$. An enlarged view (Fig. 11 right) gives details of particles position and their arrangement into traces with unique arrangement, similar to the template of light pulses. The illustration also shows the example of a few particles taken for the neighborhood analysis. Clearly a spherical search region conservatively admits a larger number of particles in the set for the analysis. The minimum radius can be put to half of the expected traveled distance. As a result, only when the particle sample in the middle of the trace is considered, the trace can be fully comprised and detected (green shaded circle). Instead, when particle samples at the edge of the trace are considered, the search will fail (red shaded circle). It can be easily seen that any a priori knowledge of the local velocity will significantly reduce the search volume and the corresponding number of particle samples included in the analysis (green shaded rectangle).

An illustration of the detection process is given in Fig. 13, where particles are displayed along the velocity vector (top left), as obtained from the time-resolved analysis of STB. The velocity vector information, however, is not used in the detection process here. When the particle samples at the edge of the trace are considered, the search region does not include the entire trace and most detections fail (top right). For samples inside the trace, depending on the local velocity, some sets return a correct trace or a spurious one (bottom left). Finally, the particle samples close to the trace midpoint mostly include the full set of samples comprised in the trace and return a correct measurement (bottom right).

When the trace rank N is increased, the probability of erroneously detection further decreases as a result of the increased uniqueness of the sequence. This aspect can be regarded as the analogous of increasing the number of particle tracers in the correlation window for PIV analysis, known to increase the SNR of cross-correlation. However, adding more pulses to the sequence has two important shortcomings: (1) the overall number of particle images in the recording increases and the probability of ghost particles with it; and (2) adding pulses and increasing the total time of the sequence increase exponentially the computational burden associated with a large search region for the trace.

The number of pulses is varied from 3 to 6 adopting a simple rule for the time separation, which increases linearly between pulses. This is realized by skipping frames from the time-resolved sequence. The case with $N=3$ considers frames 0, 1 and 3. Furthermore, for $N=4$, frames 0, 1, 3 and 6 are considered. The longest sequence ($N=6$) has been taken with a different rule for the time separation, which avoids the excessive length of the trace and at the same time gives an indication of the effect of N maintaining the same traveled path as for the case $N=5$.

The corresponding pulse time and their separation are given in the first rows of Table 3. The original single-exposure recordings feature approximately a density of particle images of 0.02 particles-per-pixel (ppp). Therefore, the density of particle images for the ME recordings is obtained multiplying the single-exposure value by the number of exposures N . The detection criterion (box j in Fig. 8) has been set conservatively at $\text{SNR} > 100$. Varying this threshold in the range 30 to 300 has shown not to bring considerable differences in the results.

The number of detected particles N_p in the measurement domain is approximately 1360, corresponding to the trajectories identified with STB. When considering multiple exposures, the number of particle samples increases linearly with

N . The number of traces detected by the current algorithm is given as a function of the number of pulses N comprised in the sequence. The relative detection rate is defined as the number of detected traces compared to those returned by the STB algorithm applied to the time-resolved single-exposure recordings.

The results indicate that for the minimum trace, composed of three samples, a relatively high rate of detection is obtained (81%), with the number of spurious detections amounting to 5.6%. Increasing the number of pulses to 4 yields a significant benefit in terms of reliability, with the error rate dropping below 1%. The detection rate, however, also reduces to 68%. Further increases in the exposures involve more computations. Yet, the detection rate declines to a minimum of 60% for $N=6$ and a negligible error rate (0.1%). The latter effect is ascribed to the hypotheses of constant velocity, at the basis of the detection criterion. As discussed before, dynamic thresholding and/or multi-pass interrogation are expected to solve or mitigate for these effects, but their implementation and assessment is considered beyond the current scope.

7 Algorithm accelerators

One of the challenges of the proposed methodology is the computational burden associated to the combinatorial nature of the trace detector. The requirements quickly increase when considering more exposures due to the associated larger neighborhood search radius, the number of trace candidates (Eq. 8) and time-tag permutations.

7.1 Non-isotropic search region

An effective technique to mitigate the computational requirements is the use of a velocity predictor to adapt the search

Table 3 Settings of ME recording and summary of results from the experimental database

N	3	4	5	6
Frame index I_F	0–1–3	0–1–3–6	0–1–3–6–10	0–1–3–6–7–10
ΔI_F	1–2	1–2–3	1–2–3–4	1–2–3–1–3
Time [ms]	0–0.33–1.0	0–0.33–1.0–2.0	0–0.33–1.0–2.0–3.3	0–0.33–1.0–2.0–2.33–3.3
i_{ppp}	0.06	0.08	0.1	0.12
iiN_p	4147	5233	6814	8176
N_{traces} (TR-STB)	1370	1358	1363	1362
N_{traces} (ME-PTV)	1144	926	861	826
Detection rate	81%	68%	63%	60%
iii Erroneous	62	27	2	1
Error rate	5.6%	2.9%	0.3%	0.1%

ⁱBased on estimated $\text{ppp} = 0.02$ from single exposure (Hendriksen et al. 2024)

ⁱⁱNumber of detected particle exposures, based on TR-STB

ⁱⁱⁱCriterion for erroneous trace $\text{Err}_U > 0.3 V_\infty$

region around a particle sample, as sketched in Figs. 12, 14—left: three-pulse sequence temporal template and the corresponding trace (bottom); middle: search region and neighborhood around the selected mark; right: linear fit evaluation of all trace possibilities, with the residuals shown in red; and right: where an elongated shape (along the local flow direction) may be considered, instead of the isotropic search radius. The use of a predictor would require an iterative implementation of the method, which is subject to further research.

7.2 Linear fit pre-selector

Besides the use of a predictor, two different strategies have been explored to reduce the cost of the candidate trace selection (box *g* in Fig. 5) and time-tag permutation (box *h*), respectively. The first approach consists of preselecting a particle trace based on their straight alignment, evaluated with a least squares linear fit (*linear fit pre-selector*). Assuming that M marks fall within the search region around the selected mark, the combinations with $N-1$ candidate marks are considered. (Each group of N marks includes the selected mark.) The set with the lowest residual is considered as candidate trace and undergoes the time-tag permutation analysis. This simplifies the evaluations of the detectability criteria from Q possibilities (Eq. 8) to P evaluations (Eq. 7) of the linear fit followed by $N!$ time-tag permutations. The approach is illustrated in Fig. 14 for a three-pulse sequence.

7.3 Direction regularity

A lighter and computationally less intensive version of the TR criterion is based on the principle that a particle does not invert the direction of motion within the trace. Once a candidate trace has been selected, the time-tag permutation analysis (blok *h*) can be simplified by restricting the search only to those combinations where the velocity direction between subsequent illuminations does not vary beyond 90 degrees. The latter is considered a conservative criterion, considering that for most cases, a spurious time-tag permutation results in displacement reversal along the trace. The operation is computationally efficient, considering that the trajectory has been approximated as rectilinear and the criterion is coded as sign reversal detection (dot product of

subsequent displacement vectors, Fig. 15). The result yields only two possible permutations (instead of $N!$). The two candidates are then inquired with the composite detection criterion, as illustrated in the last column of Fig. 15, for a three-pulse sequence.

7.4 Computational effort

The effect of the above accelerators in terms of computational effort is summarized in Table 4, by comparing the CPU time required to evaluate the recordings. The analysis compares the trace detection criterion with and without the linear fit pre-selector followed by the direction regularity. All computations have been performed in a workstation equipped with an Intel Xeon W-2223 CPU running a MATLAB script (without parallelization of the computation). A simplified version of the script and a sample of the data used for the present study are provided as supplementary material.

The results indicate rapidly increasing computational burden with trace length/rank when the evaluation makes no use of accelerators. The linear fit pre-selector provides already a strong reduction of the number of combinations, resulting in a substantial reduction of the computational effort for the longer traces. Finally, the one-directional time tag brings a modest reduction of computational effort, yet appreciable for the longer sequences. It must be noted that the additional restrictions posed by the accelerators (straight trajectory, no direction reversal) may not hold true in highly turbulent regions, where the tracers follow highly curved trajectories. This may increase the occurrence of false negatives (missed detections) of such trajectories. Still, the accelerators represent a powerful tool to produce a first estimate of the velocity field, for use as a predictor in an iterative algorithm.

8 Potential and bottlenecks of ME-PTV

Several aspects deserve attention for the further pursuit of this technique. The main positive points are that the use of traces from ME recordings significantly lowers hardware requirements: The ME-PTV does not require high-speed imagers, neither short interframe separation time. It is therefore expected that experiments can be conducted using ordinary single-frame monochrome cameras.

A second positive aspect is the reduction of data storage, as the velocity measurement is based on a single image. Furthermore, the free choice of the number of exposures N also allows to tune the information density on each image.

Finally, when compared with double frame single exposure, traces of 3 or more exposures offer a higher

Table 4 CPU time required for trace detection of one recording from the experimental database

N	3 (s)	4 (s)	5	6
TD (no accelerators)	0.3	3	14 h	> 1 day
Linear fit pre-selector	0.3	1	1 min	15 min
Linear fit + directional regularity	0.2	0.5	20 s	3 min

measurement dynamic range (Novara et al. 2023), which compares to state-of-the-art techniques based on time-resolved single-exposure recordings (e.g., STB).

Among the most problematic aspects of this technique is that of particle images overlapping in regions with declining velocity. The current technique fails to detect traces under such conditions, and additional criteria will be needed for the treatment of low-to-zero velocity conditions. A second point of attention is the limit of seeding concentration: The ME recording multiplies the number of particle images in a single recording, and as such, it aggravates the problem of ghost particles formation. This aspect can be mitigated with the use of a multitude of cameras (e.g., $N_{\text{cam}} > 10$) such as practiced in studies that require redundancy of imaging directions.

9 Conclusions

A novel measurement approach is proposed, to analyze the 3D motion of particle tracers, based on multi-exposed recordings (ME-PTV). Irregular timing of illumination produces unique patterns, or *traces* from particle images, with a specific, asymmetric pattern. The latter is easy to recognize and solves for the well-known problem of directional ambiguity hampering single-frame recording techniques. The detection of a trace from a group of particle samples is based on kinematic similarity (KS) and reinforced with a trace regularity (TR) criterion that penalizes particle acceleration. Altogether these two criteria allow identifying traces from clusters of 3D particle samples. A signal-to-noise ratio (SNR) is introduced, which implements the criterion for trace detection. The latter yields relatively high values (10–100) for traces where the velocity varies within 20% of the mean value.

The assessment based on an experimental database shows a maximum detection rate above 80% for the lowest number of exposures ($N=3$), declining to approximately 60% for $N=6$. Conversely, the error rate decreases from 6 to 0.1%, respectively, with more than 90% of the detected traces exhibiting $\text{SNR} > 100$, indicating the robustness of the composite detection criterion.

The computational effort limits the sequence length due to the combinatorial approach to trace detection. It is concluded that traces with 3 to 4 pulses guarantee a high detection rate and error probability in the order of 1%. Finally, the lower limit of measurable velocity is hampered by

overlapping particle images, which solution is left open to further research.

Supplementary Information The online version contains supplementary material available at <https://doi.org/10.1007/s00348-025-03993-3>.

Acknowledgements The experimental database has been made available from an experiment conducted by Luuk Hendriksen, who is kindly acknowledged.

Author Contribution F.S. and I.H. wrote the main manuscript text. A.G.G prepared figures, graphical material and pseudocode. All authors reviewed the manuscript.

Data availability No datasets were generated or analyzed during the current study.

Declarations

Conflict of interest The authors declare no competing interests.

Open Access This article is licensed under a Creative Commons Attribution 4.0 International License, which permits use, sharing, adaptation, distribution and reproduction in any medium or format, as long as you give appropriate credit to the original author(s) and the source, provide a link to the Creative Commons licence, and indicate if changes were made. The images or other third party material in this article are included in the article's Creative Commons licence, unless indicated otherwise in a credit line to the material. If material is not included in the article's Creative Commons licence and your intended use is not permitted by statutory regulation or exceeds the permitted use, you will need to obtain permission directly from the copyright holder. To view a copy of this licence, visit <http://creativecommons.org/licenses/by/4.0/>.

References

- Adrian RJ, Westerweel J (2011) Particle image velocimetry. Cambridge University Press, Cambridge, UK
- Agüí JC, Jimenez J (1987) On the performance of particle tracking. *J Fluid Mech* 185:447–468
- Bosbach J, Kühn M, Wagner K (2009) Large scale particle image velocimetry with helium filled soap bubbles. *Exp Fluids* 46:539–547
- Cierpka C, Kähler CJ (2012) Cross-correlation or tracking—comparison and discussion. In: 16th international symposium on applications of laser techniques to fluid mechanics. Lisbon, Portugal
- Grant I, Liu A (1990) Directional ambiguity resolution in particle image velocimetry by pulse tagging. *Exp Fluids* 10:71–76
- Hendriksen LA, Sciacchitano A, Scarano F (2024) Object registration techniques for 3D particle tracking. *Meas Sci Technol* 35:125202
- Hysa I, Tuinstra M, Sciacchitano A, Scarano F, van der Meulen MJ, Rockstroh T, Roosenboom EWM (2024) A multi-directional redundant 3D-LPT system for ship–flight–deck wind interactions. *Exp Fluids* 65:126
- Hysa I, Scarano F, Sciacchitano A, Tuinstra M (2022) Time-space correlation of multiple-exposure PTV with incommensurable

- intervals, In: 20th international symposium on applications of laser and imaging techniques to fluid mechanics. Lisbon, Portugal
- Jux C, Sciacchitano A, Scarano F (2020) Flow pressure evaluation on generic surfaces by robotic volumetric PTV. *Measur Sci Technol* 31(10):104001
- Kähler CJ, Scharnowski S, Cierpka C (2012a) On the uncertainty of digital PIV and PTV near walls. *Exp Fluids* 52:1641–1656
- Kähler CJ, Scharnowski S, Cierpka C (2012b) On the resolution limit of digital particle image velocimetry. *Exp Fluids* 52:1629–1639
- Keane RD, Adrian RJ (1992) Theory of cross-correlation analysis of PIV images. *Appl Sci Res* 49:191–215
- Lynch K, Scarano F (2013) A high-order time-accurate interrogation method for time-resolved PIV. *Meas Sci Technol* 24:035305
- Maas HG, Gruen A, Papantoniou D (1993) Particle tracking velocimetry in three-dimensional flows, Part 1. Photogrammetric determination of particle coordinates. *Exp Fluids* 15:133–146
- Malik NA, Dracos TH (1993) Lagrangian PTV in 3D flows. *Appl Sci Res* 51:161–166
- Novara M, Schanz D, Geisler R, Gesemann S, Voss C, Schröder A (2019) Multi-exposed recordings for 3D Lagrangian particle tracking with multi-pulse shake-the-box. *Exp Fluids* 60:1–19
- Novara M, Schanz D, Schröder A (2023) Two-pulse 3D particle tracking with shake-the-box. *Exp Fluids* 64:93
- Qureshi MH, Tien W-H (2022) Novel streak-resolving algorithm for particle streak velocimetry. *Flow Meas Instr* 87:102208
- Raffel M, Willert CE, Scarano F, Kähler CJ, Wereley ST, Kompenhans J (2018) Particle image velocimetry—a practical guide. Springer-Verlag, Heidelberg, DE
- Roosenboom EWM, Jux C, Sciacchitano A, Scarano F (2020) Flow pressure evaluation on generic surfaces by robotic volumetric PTV. *Meas Sci Technol* 31:104001
- Saredi E, Sciacchitano A, Scarano F (2020) Multi- Δt 3D-PTV based on Reynolds decomposition. *Measur Sci Technology* 31(8):084005
- Schanz D, Gesemann S, Schröder A (2016) Shake the box: Lagrangian particle tracking at high particle image densities. *Exp Fluids* 57:1–27
- Utami T, Ueno T (1984) Visualization and picture processing of turbulent flow. *Exp Fluids* 2:25–32
- Wieneke B (2012) Iterative reconstruction of volumetric particle distribution. *Meas Sci Technol* 24:024008
- Wieneke B, Rockstroh T (2024) Lagrangian particle tracking in the presence of obstructing objects. *Meas Sci Technol* 35:055303
- Willert C, Stasicki B, Klinner J, Moessner S (2010) Pulsed operation of high-power light emitting diodes for imaging flow velocimetry. *Meas Sci Technol* 21:075402
- Zhang D, Tropea C, Zhou W, Cai T, Huang H, Dong X, Gao L, Cai X (2024) Particle streak velocimetry: a review. *Exp Fluids* 65(9):130

Publisher's Note Springer Nature remains neutral with regard to jurisdictional claims in published maps and institutional affiliations.